

Sensitivity test of parameterizations of subgrid-scale orographic form drag in the NCAR CESM1

Yishuang Liang^{1,4} · Lanning Wang^{1,4} · Guang Jun Zhang^{2,3} · Qizhong Wu^{1,4}

Received: 30 September 2015 / Accepted: 11 July 2016 / Published online: 10 August 2016
© Springer-Verlag Berlin Heidelberg 2016

Abstract Turbulent drag caused by subgrid orographic form drag has significant effects on the atmosphere. It is represented through parameterization in large-scale numerical prediction models. An indirect parameterization scheme, the Turbulent Mountain Stress scheme (TMS), is currently used in the National Center for Atmospheric Research Community Earth System Model v1.0.4. In this study we test a direct scheme referred to as BBW04 (Beljaars et al. in *Q J R Meteorol Soc* 130:1327–1347, 2004. doi:10.1256/qj.03.73), which has been used in several short-term weather forecast models and earth system models. Results indicate that both the indirect and direct schemes increase surface wind stress and improve the model's performance in simulating low-level wind speed over complex orography compared to the simulation without subgrid orographic effect. It is shown that the TMS scheme produces a more intense wind speed adjustment, leading to lower wind speed near the surface. The low-level wind speed by the BBW04 scheme agrees better with the ERA-Interim reanalysis and is more sensitive to complex orography as a direct method. Further, the TMS scheme increases the 2-m temperature and planetary boundary layer height over large areas of tropical and subtropical Northern Hemisphere land.

Keywords Subgrid-scale · Turbulent form drag · Parameterization schemes · Community earth system model

1 Introduction

The earth's orography affects the atmosphere both dynamically and thermodynamically, and contributes significantly to the global pattern of the atmospheric circulation and climate systems. Airflow can be influenced by the undulation, gradient, exposure, anisotropy, and horizontal scale of orography. Orography can be divided into large-scale and subgrid-scale in a global climate model (GCM). Large-scale orography (e.g. the Tibetan Plateau and the Rocky Mountains) affects the atmosphere through forced uplift, mountain waves, blocking, and diffluence. Subgrid-scale orography can induce surface drag due to inhomogeneity in topographic features. Drag can be related to (1) gravity waves produced by over-the-mountain flow, (2) blocking and splitting of the low-level flow, and (3) turbulent drag caused by form drag exerted by subgrid obstacles. This study mainly focuses on turbulent orographic form drag from subgrid-scale orography.

Research on turbulent orographic form drag began when Jackson and Hunt (1975) developed a linear theory of over-the-mountain turbulence under neutral stratification. They related changes in wind speed and stress to the size and shape of hills and the roughness of the surfaces involved. Sykes (1980) and Hunt et al. (1988) used asymptotic analyses to explore the mechanism of the turbulent orographic form drag and described the linear changes of turbulent boundary layer flow over a low hill. Belcher et al. (1993) improved upon the earlier work of Hunt et al. (1988) and suggested that, under neutral stratification,

✉ Lanning Wang
wangln@bnu.edu.cn

¹ College of Global Change and Earth System Science, Beijing Normal University, Beijing 100875, China

² Scripps Institution of Oceanography, La Jolla, CA, USA

³ Center for Earth System Science, Tsinghua University, Beijing 100084, China

⁴ Joint Center for Global Change Studies, Beijing 100875, China

turbulent orographic form drag is generated by what they called “non-separated sheltering effect”. Wood and Mason (1993) used numerical methods and discussed turbulent drag over small-scale hills under neutral conditions. Later, using analytical and numerical models Belcher and Wood (1996) suggested that the turbulent drag over low hills could be quite significant (even more than surface friction) in weakly stable or neutral flow, but it will be reduced as the stratification becomes more stable. Brown and Wood (2003) assessed the ability of effective roughness length parameterization in numerical models to represent the effects of the subgrid hills in stable conditions while Allen and Brown (2006) discussed it in convective conditions.

While numerical models can resolve large-scale orographic effects, with limited model resolution, they can only represent subgrid-scale orography through parameterization. For subgrid turbulent orographic form drag, the parameterization can be categorized into indirect and direct methods. The effective roughness length scheme, an indirect method, is widely used to represent subgrid turbulent orographic form drag (e.g. Wood and Mason 1993; Brown and Wood 2003; Allen and Brown 2006; Richter et al. 2010). Fiedler and Panofsky (1972) defined the effective roughness length as the roughness length for heterogeneous terrain that would yield the same surface wind stress as the roughness length for homogenous terrain. The effective roughness length method assumes that the undulation of orography increases surface roughness. The roughness length increases beyond its original vegetative value, so that the total surface drag (including the original turbulent friction and the subgrid turbulent drag) is represented as

$$F_{tot} = F_p + F_t, \quad (1)$$

where F_p and F_t are the turbulent drag and friction stress, respectively. The concept of an indirect method signifies that this turbulent drag is felt by the model through changing the surface turbulent momentum flux in the boundary layer.

Wood et al. (2001, hereafter referred to as WBH01) first proposed a direct parameterization scheme, which considered the subgrid turbulent orographic form drag as a dynamic forcing term in the equation of atmospheric motion instead of an increase of roughness length. They suggested that WBH01 scheme is at least as good as the effective roughness length scheme in neutral condition. Rontu (2006) simplified the WBH01 scheme and used it in the high-resolution limited area model (HIRLAM). However, WBH01 only considered a simple case of flow over an infinite series of sinusoidal ridges, and did not address the issue of multiple scales of complex real orography for large-scale models (Beljaars et al. 2004). Beljaars et al. (2004) proposed a new scheme (referred to as BBW04 hereafter), which was based on the formulation of Wood

and Mason (1993), using the vertical attenuation from WBH01 and the parameterized orographic spectrum. It too considers form drag as a term in the equation of atmospheric motion. Furthermore, It suggested using subgrid scales above 5000 m for gravity wave and low-level blocking parameterizations and considering orography scales smaller than 5000 m for turbulent form drag.

The effective roughness scheme has been used in several numerical weather prediction models (e.g. Wilson 2002; Webster et al. 2003) and climate models (e.g. Community Earth System Model, CESM1.0.4), and has significantly improved the model performance (e.g. Milton and Wilson 1996; Lindvall et al. 2013). The BBW04 scheme was tested and used in the European Centre for Medium range Weather Forecasting (ECMWF) numerical weather prediction (NWP) model (Beljaars et al. 2004) and Earth System model EC-EARTH’s atmospheric model IFS (IFS DOCUMENTATION–cy41r1 2015), and the Chinese Global and Regional Assimilation and Prediction System (Xue et al. 2011) for weather prediction. According to the work by Wood et al. (2001) and Beljaars et al. (2004), the direct scheme BBW04 has several advantages in the ECMWF model compared with the effective roughness scheme. First, the essential difference between the two schemes is that subgrid form drag is incorporated directly into the momentum equation in BBW04, instead of being treated as an increase of surface roughness length. Form drag is considered as a dynamic effect, about which the BBW04 scheme is more explicit and theoretically consistent than the effective roughness length scheme. It is no longer necessary to consider the compensation of the roughness lengths of heat and moisture. Second, the scales of orography are taken into account in ECMWF, which makes the distinction of subgrid parameterizations more specific. Also, only the effects due to horizontal scales smaller than 5000 m are considered as turbulent form drag, and the rest are considered for gravity wave and low-level blocking in their model. Third, the direct scheme BBW04 is less affected by stability while the effective roughness length scheme can interact very strongly with boundary-layer stability.

In this study, we test the BBW04 scheme in NCAR’s climate model CESM1.0.4 to determine its feasibility and performance for global climate models. Section 2 describes the model setup and data used for evaluation. Section 3 presents the results, and Sect. 4 summarizes the paper.

2 Model, form drag parameterization and data

This study uses the NCAR’s Community Earth System Model (Hurrell et al. 2013) version 1.0.4. It consists of five component models, the Community Atmosphere Model

version 5 (CAM5; Neale et al. 2010), the Community Land model version 4 (CLM4; Lawrence et al. 2011), the Los Alamos National Laboratory (LANL) Community Ice Code (CICE4; Hunke and Lipscomb 2008), the Parallel Ocean Program version 2 (POP2; Smith et al. 2010) and a coupler CPL7 (Gent et al. 2011). The CAM5 uses a horizontal resolution $0.9^\circ \times 1.25^\circ$ (latitude \times longitude) and 30 vertical levels, with finite-volume dynamic core and a time step of 1800 s. Note that, different from the work in Wood et al. (2001) and Beljaars et al. (2004) in the ECMWF model, gravity wave drag in CAM5 acts upon all subgrid scales. Also, low-level blocking parameterization is not included in current CAM5. CLM4 has the same horizontal resolution as CAM5. The ocean and sea-ice modules use climatological sea surface temperature and sea ice data.

2.1 Parameterization schemes

2.1.1 An indirect parameterization scheme—TMS scheme

In the CESM1.0.4 model, the turbulent drag from subgrid-scale orography is represented by the Turbulent Mountain Stress (TMS) scheme using effective roughness length within the model physics package (Neale et al. 2010). In the original TMS scheme, the roughness length z_0^{SSO} (super-script SSO denotes subgrid-scale orography) is calculated using the standard deviation σ of subgrid-scale terrain height

$$z_0^{SSO} = 0.075\sigma. \quad (2)$$

The additional wind stress due to TMS is calculated as:

$$\boldsymbol{\tau} = \rho |\mathbf{V}| \mathbf{V} \frac{f(R_i) \kappa^2}{\ln^2 \left(\frac{z+z_0^{SSO}}{z_0^{SSO}} \right)}, \quad (3)$$

where ρ is air density, \mathbf{V} is the horizontal wind vector of the lowest model layer, κ is von Karman's constant, z is the height above the surface, and $f(R_i)$ is a function of the Richardson number: $f(R_i) = 1$ if $R_i < 0$; $f(R_i) = 0$ if $R_i > 1$; and $f(R_i) = 1 - R_i$ if $0 < R_i < 1$ (Richter et al. 2010).

The wind stress calculated by Eq. (3) is added to the model's planetary boundary layer (PBL) scheme to evaluate the vertical transport. It is employed only in grid cells where the topography is above the sea level (Neale et al. 2010).

In CAM5 the TMS scheme is used to correct the total surface drag coefficient k_{tot} when calculating the surface momentum flux, rather than providing the drag stress enhancement caused by subgrid orography. k_{tot} is computed by summing the normal drag coefficient k_{nor} and the turbulent mountain stress drag coefficient k_{tms} , which is obtained from the TMS scheme,

$$k_{tms} = \rho |\mathbf{V}| \frac{f(R_i) \kappa^2}{\ln^2 \left(\frac{z+z_0^{SSO}}{z_0^{SSO}} \right)}, \quad (4)$$

$$k_{tot} = k_{nor} + k_{tms}. \quad (5)$$

The adjusted total surface drag coefficient k_{tot} is then used to calculate the momentum flux in the lowest model layer, and influences the wind profiles in the upper layers through the vertical diffusion process. Meanwhile, as the transfer of heat and moisture between the lowest model level and the surface is hardly affected by subgrid orography effects (Beljaars et al. 2004), heat and moisture fluxes are not adjusted by TMS scheme.

2.1.2 A direct parameterization scheme—BBW04 scheme

In the direct parameterization scheme, BBW04 considers the subgrid turbulent orographic form drag as a forcing term in the equation of atmospheric motion

$$\frac{\partial \mathbf{V}}{\partial t} = \left(\frac{\partial \mathbf{V}}{\partial t} \right)_d + \left(\frac{\partial \mathbf{V}}{\partial t} \right)_p, \quad (6)$$

where $\left(\frac{\partial \mathbf{V}}{\partial t} \right)_d = -\frac{1}{\rho} \nabla p - 2\boldsymbol{\Omega} \times \mathbf{V} + \mathbf{g} + \mathbf{F}$ is from the atmospheric dynamics, and $\left(\frac{\partial \mathbf{V}}{\partial t} \right)_p = -\frac{1}{\rho} \frac{\partial \boldsymbol{\tau}}{\partial z}$ is from parameterized physics. $\boldsymbol{\tau} = \sum_i \boldsymbol{\tau}_i$ is the sum of the momentum fluxes from different physical processes, including subgrid-scale orographic effect. Here, the parameterization of turbulent orographic form drag is $\frac{1}{\rho} \frac{\partial \boldsymbol{\tau}_{SSO}}{\partial z}$.

The BBW04 parameterization scheme is expressed as follows:

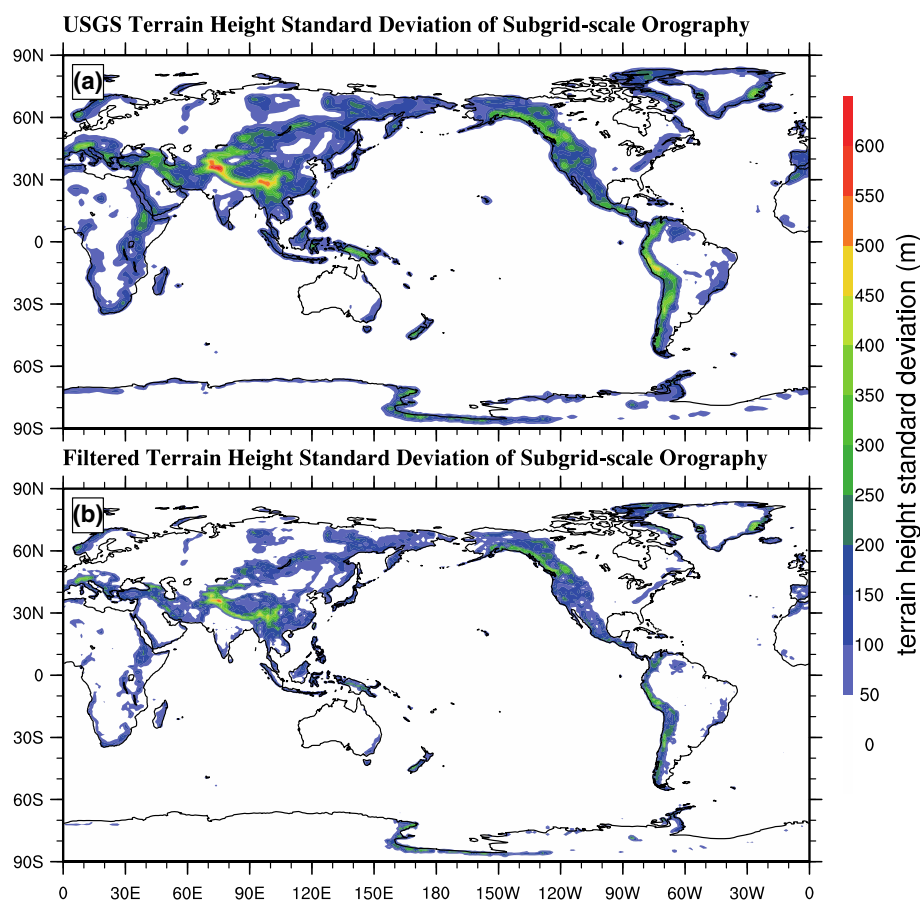
$$\frac{1}{\rho} \frac{\partial \boldsymbol{\tau}_{SSO}}{\partial z} = \alpha \beta C_{md} C_{corr} |\mathbf{V}(z)| \mathbf{V}(z) 2.109 e^{-(z/1500)^{1.5}} a_2 z^{-1.2}, \quad (7)$$

where $\alpha = 12$ is a shear-dependent parameter, $\beta = 1$ is the shape factor, $C_{md} = 0.005$ and $C_{corr} = 0.6$ are the drag and correction coefficients, $\mathbf{V}(z)$ is the horizontal wind vector, z is the model level height, $a_2 = a_1 k_1^{n_1 - n_2}$, $a_1 = \sigma_{flt}^2 (I_H k_{flt}^{n_1})^{-1}$, $I_H = 0.00102 \text{m}^{-1}$, $k_{flt} = 0.00035 \text{m}^{-1}$, $n_1 = -1.9$, $n_2 = -2.8$, and σ_{flt} is the filtered terrain height standard deviation of subgrid orography. It is incorporated and solved in the model's dynamic steps since it adds the effects of subgrid turbulent drag into the momentum equation. The calculated wind velocity is used directly in the next physics step.

2.2 Data

The input data needed for the model simulation is from the NCAR CESM input files for the CESM1.0.4 model.

Fig. 1 Two sets of terrain height standard deviation data of subgrid-scale orography at $0.9^\circ \times 1.25^\circ$ (latitude \times longitude) resolution: **a** the USGS topographic data; **b** the filtered terrain height standard deviation data



Note that the TMS and the BBW04 scheme both require standard deviation data of subgrid orography terrain height with the same resolution as the model. TMS uses US Geological Survey (USGS) topographic data, while BBW04 uses filtered terrain height standard deviation data. Following Beljaars et al. (2004), we apply a band-pass filter to the global $30''$ terrain height field twice, and the standard deviation of the terrain height is then computed from the filtered field. First, terrain heights with horizontal scales <2 km or greater than 20 km are filtered. Second, the standard deviation of the filtered terrain height within each $5 \text{ km} \times 5 \text{ km}$ box is computed because BBW04 only acts on scales below 5000 m. Figure 1 shows the standard deviation of subgrid orography terrain height for both unfiltered and filtered data. The filtered terrain height standard deviation data have smaller values and are smoother than the original data. For instance, with a horizontal resolution of $0.9^\circ \times 1.25^\circ$, the filtered terrain height standard deviation is on average 1.17 % smaller (12.28 m) than that of the USGS data.

The model simulations are evaluated against global reanalysis and observation datasets. The ERA-Interim reanalysis gridded data from 1979 to 2014 (Berrisford et al. 2011) with 1° horizontal resolution and 37 vertical

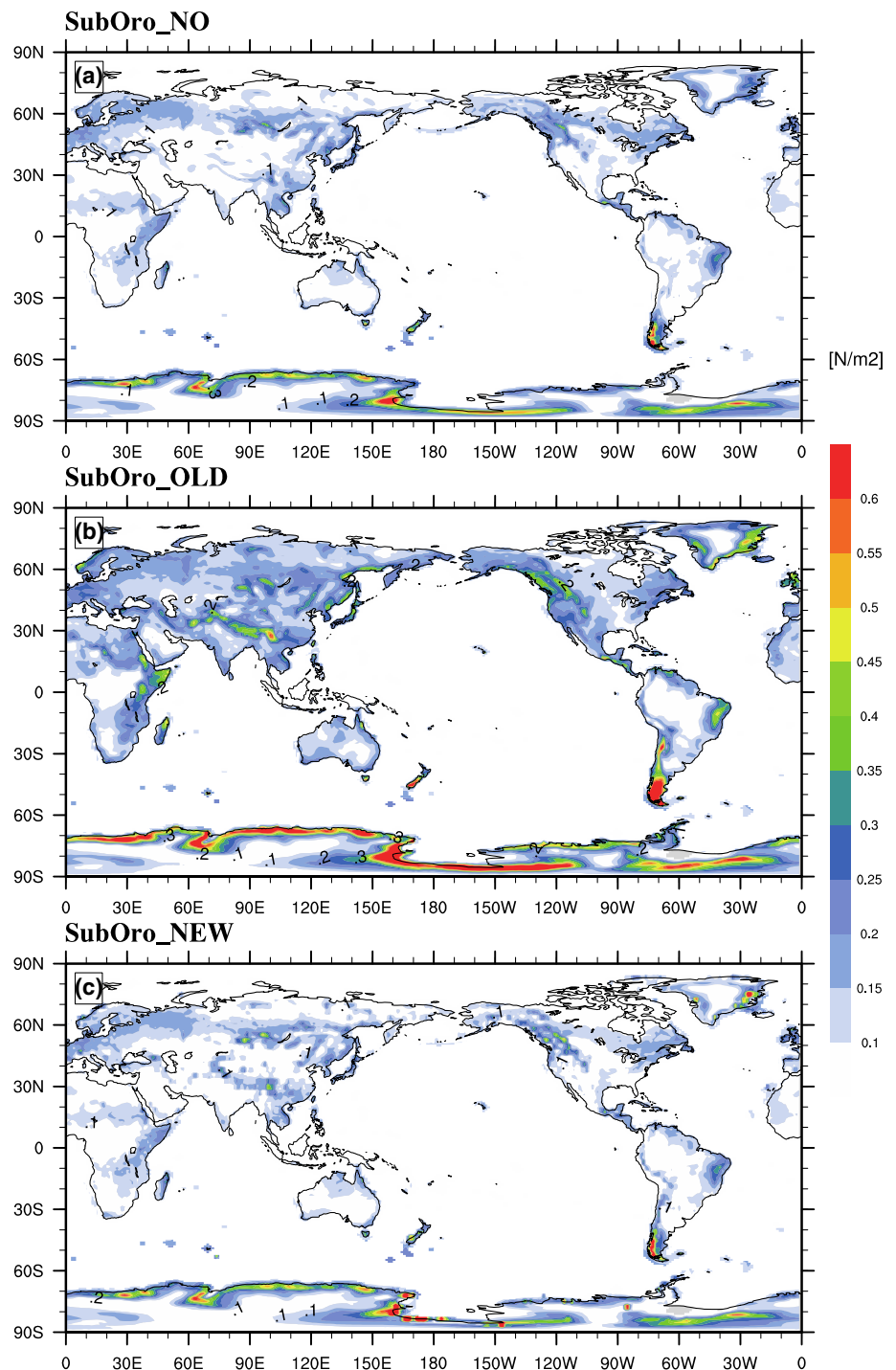
Table 1 Specification of three sets of experiments

	SubOro_NO	SubOro_OLD	SubOro_NEW
TMS	×	✓	×
BBW04	×	×	✓

✓ Scheme was activated; × scheme was not activated

levels produced by the ECMWF is used for comparing with model simulations. It is noted that the model used to produce ERA-Interim also used BBW04, which may lead to similar results when comparing low-level wind speed between ERA-Interim and the CAM5 experiment with BBW04 implemented. Therefore, two more reanalysis datasets are used to evaluate low-level wind speed: the NCEP Global Reanalysis 2 (NCEP-2) covering the years 1979–2014 with T62 resolution and the 25-yr Japanese Reanalysis (JRA25) covering the years 1979–2004 with a spectral resolution of T106. Two datasets for near-surface temperature and precipitation are included in this study: the Willmott and Matsuura dataset version 3.02 for 1950–1999 (Willmott and Robeson 1995) and the Xie-Arkin CPC Merged Analysis of Precipitation (CMAP) dataset with T42 resolution for 1979–1998 (Xie and Arkin 1997).

Fig. 2 Global annual-mean total surface wind stress over land ($\sigma > 0$) for **a** SubOro_NO; **b** SubOro_OLD and **c** SubOro_NEW



2.3 Experiments

Three sets of experiments (Table 1) were performed: SubOro_NO with no parameterization of subgrid-scale turbulent orographic form drag, SubOro_OLD with the TMS scheme used, and SubOro_NEW with the BBW04 scheme used in the model. All three runs were carried out for 20 years and the first 5 years were discarded to avoid any

spin-up. The analyses in Sect. 3 are based on the average from the last 15 years of the simulations.

3 Results and analysis

The annual mean of scalar magnitudes of wind stress from the run without subgrid orographic terrain effect

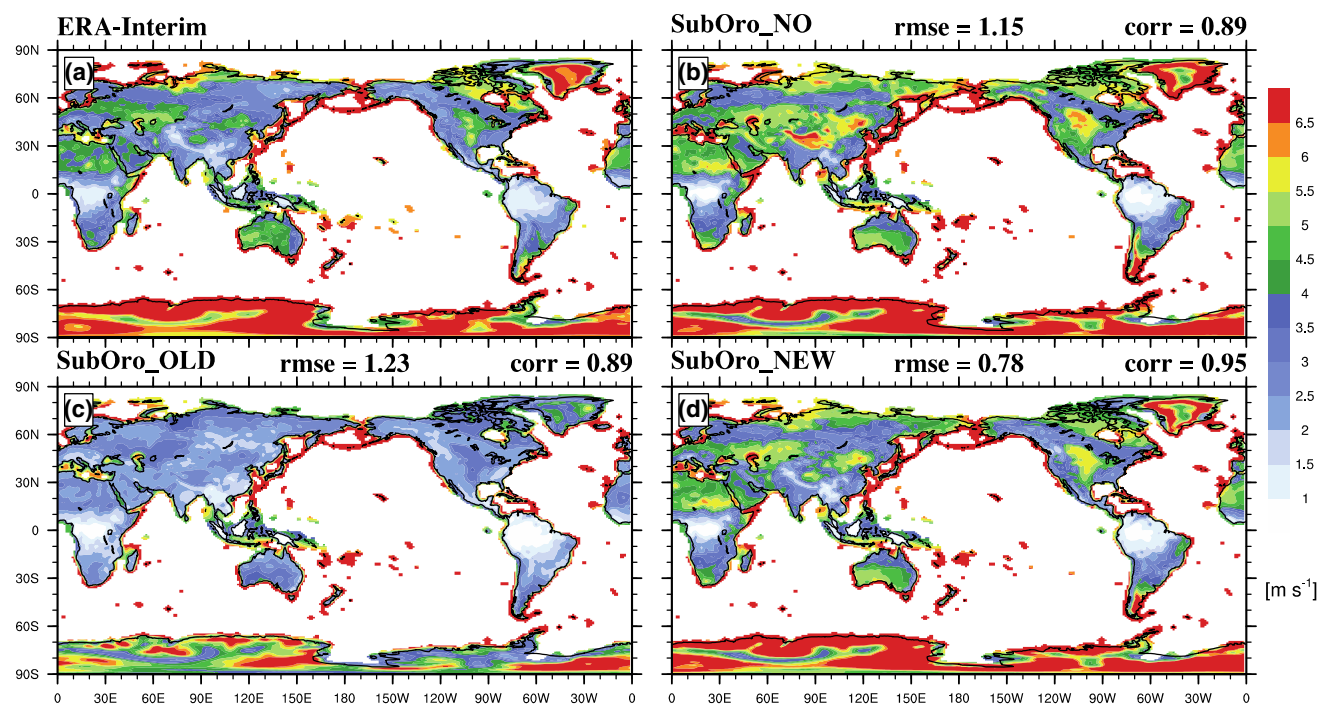


Fig. 3 Global annual-mean 10-m total wind speed over land ($\sigma > 0$) for **a** ERA-Interim reanalysis; **b** the run without subgrid orographic terrain effect (SubOro_NO); and the run using **c** indirect (SubOro_OLD) or **d** direct scheme (SubOro_NEW)

Table 2 Global averaged (weighted) 10-m wind speed of ERA-Interim, NCEP2, JAR25 and three model runs over land and ocean areas (ms^{-1})

	ERA-interim	NCEP2	JAR25	SubOro_NO	SubOro_OLD	SubOro_NEW
Land	4.80	3.54	2.10	5.23	3.93	4.93
Ocean	7.51	5.35	4.12	7.97	7.93	7.97

(SubOro_NO) and the runs using indirect (SubOro_OLD) and direct (SubOro_NEW) schemes are shown in Fig. 2. Note that in SubOro_NEW the total surface wind stress has two components, one from grid-scale surface roughness, which is directly output from the model simulation, and one from subgrid orography. The latter is obtained by integrating Eq. (7) from the surface upward to the highest model level. The wind stress differences over oceans are small. Thus, the wind stresses are only shown in regions where $\sigma > 0$. The smallest wind stress is simulated in SubOro_NO. The wind stresses over complex terrains (e.g. over the Tibetan Plateau and the Rocky Mountains) are enhanced in SubOro_OLD and SubOro_NEW, both of which implemented the subgrid drag effects, but with different magnitude. SubOro_OLD simulates stronger surface drag than SubOro_NEW.

Figure 3 shows the global annual-mean 10-m total wind speed of ERA-Interim Reanalysis (1979–2014) and the three model runs respectively. The root mean squared error (RMSE) and the pattern correlation coefficients (corr) between model runs and ERA-Interim are also presented above each plot. The 10-m wind speed is greatest in the

case of SubOro_NO. Both indirect and direct schemes reduce low-level wind speed effectively in areas where complex orography exists and wind speed is relatively high. SubOro_OLD simulates the lowest wind speed. SubOro_NEW, with the lowest RMSE and highest pattern correlation, shows the best agreement with ERA-Interim. The 10-m wind speeds of three runs are also compared with NCEP2 Reanalysis (1979–2014) and JRA25 Reanalysis (1979–2004). The averaged 10-m wind speeds of models and reanalysis are given in Table 2. The average wind speeds of three model runs are all closest to that of ERA-interim over both land and ocean areas. The RMSEs and correlation coefficients of models compared to three reanalysis data are shown in Table 3. The highest correlations and lowest RMSEs in each comparison are bolded in the table. Both SubOro_NO and SubOro_NEW have better correlation coefficients but worse RMSEs than SubOro_OLD when compared with NCEP2 and JRA25.

Figure 4 is the same as Fig. 3, but zooms into different regions to show regional scale features: Asia ($0\text{--}60\text{N}^\circ$, $60\text{--}140\text{E}^\circ$), which has the most complex orography in the

Table 3 Pattern correlation coefficients and RMSEs of model 10-m wind speed compared with reanalysis

	SubOro_NO		SubOro_OLD		SubOro_NEW	
	CORR	RMSE	CORR	RMSE	CORR	RMSE
ERA-interim	0.89	1.15	0.89	1.23	0.95	0.78
NCEP2	0.76	2.35	0.67	1.90	0.75	2.16
JRA25	0.70	3.61	0.58	2.80	0.70	3.37

Bold values indicate highest correlations and lowest RMSEs in each set

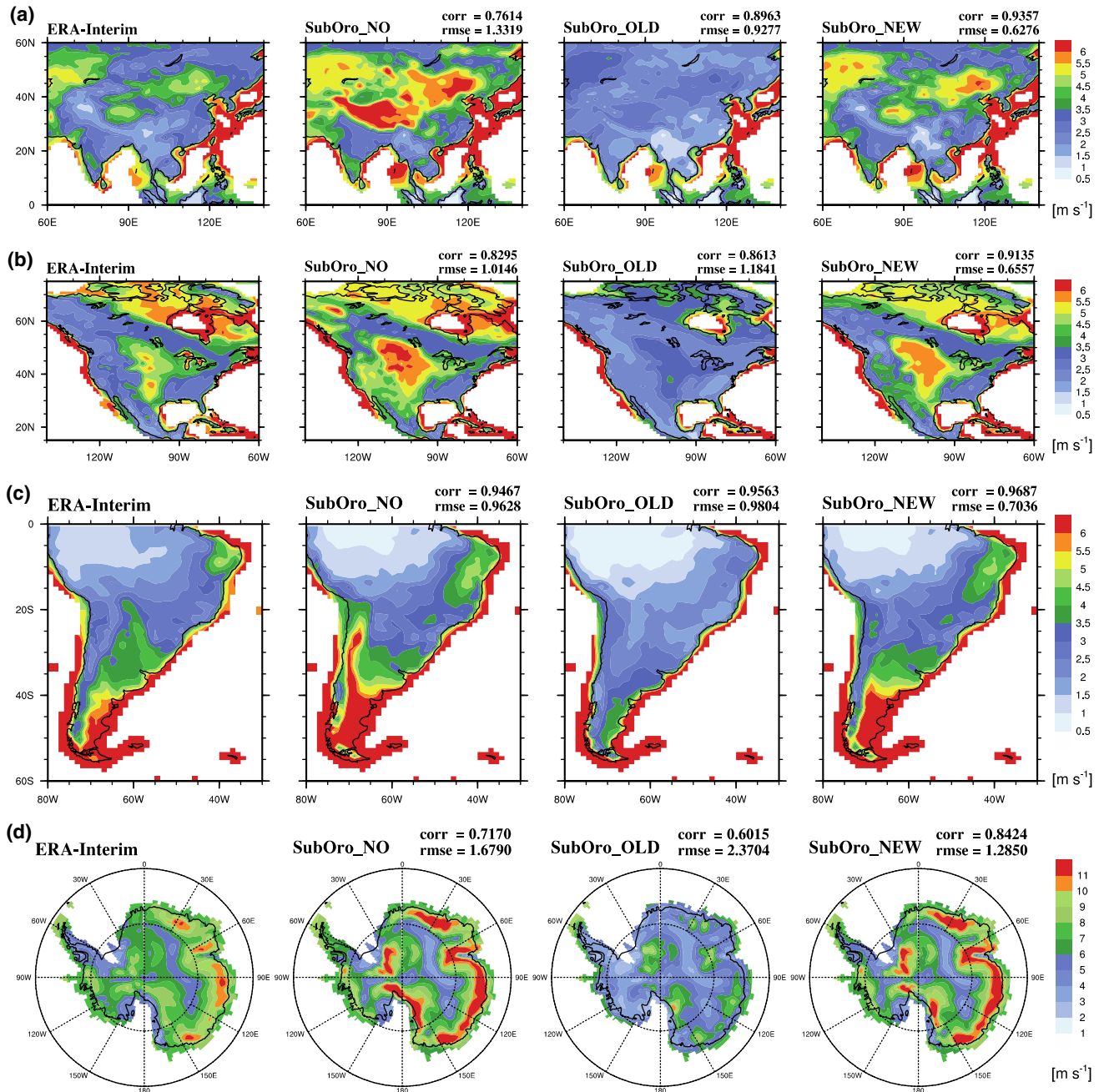
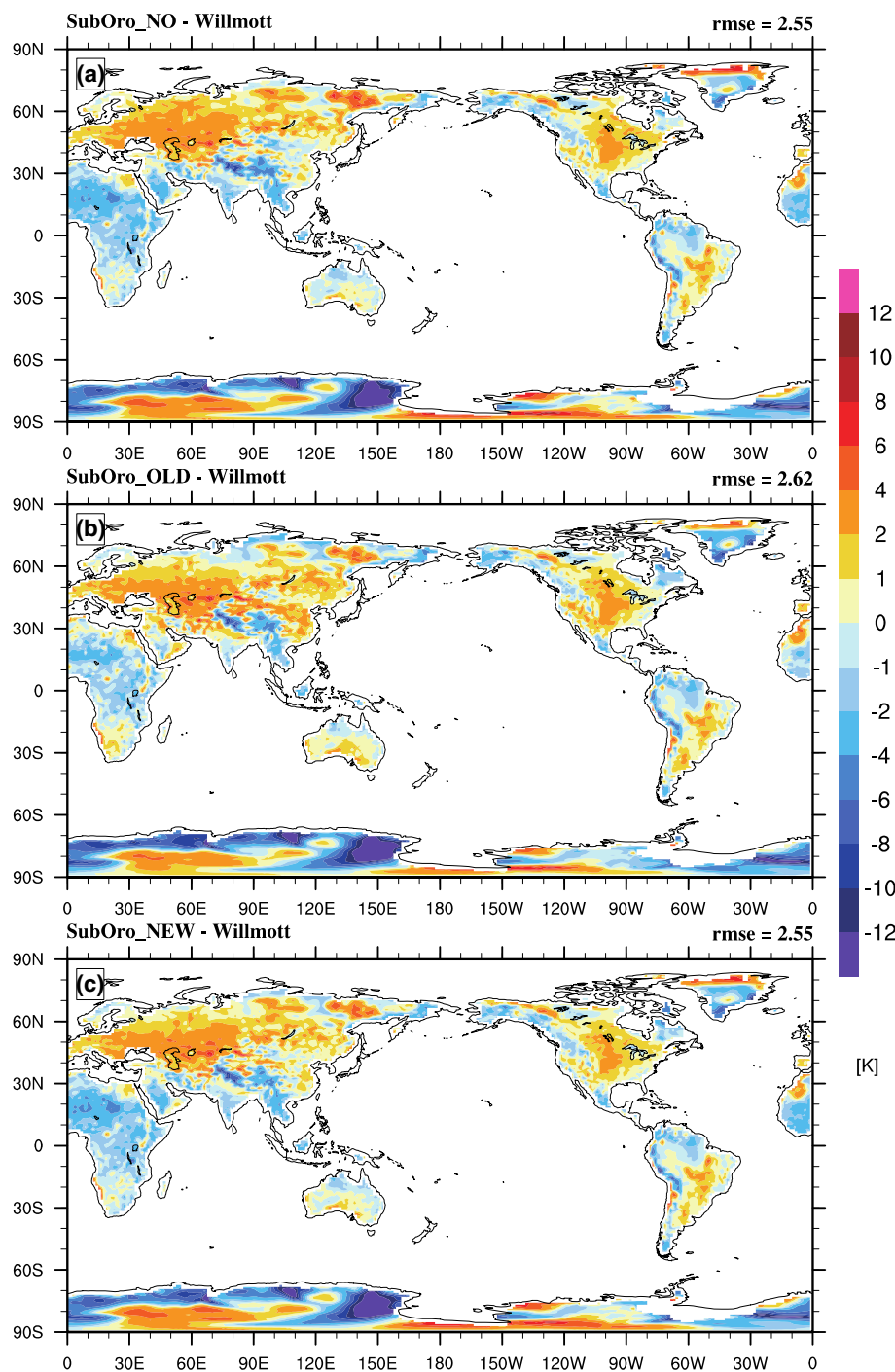


Fig. 4 As Fig. 3, but in **a** Asia ($0-60^{\circ}$, $60-140^{\circ}$); **b** North America ($15-75^{\circ}$, $60-140^{\circ}$); **c** South America ($0-60^{\circ}$, $30-80^{\circ}$); **d** Antarctica ($60-90^{\circ}$)

Fig. 5 The differences of 2-m air temperature between **a** SubOro_NO, **b** SubOro_OLD, **c** SubOro_NEW and Willmott and Matsuura surface air temperature (1950–1999) over land ($\sigma > 0$)



world due to the existence of the Tibetan Plateau (Fig. 4a); North America ($15\text{--}75\text{N}^\circ$, $60\text{--}140\text{W}^\circ$), covering Rocky Mountains (Fig. 4b); South America ($0\text{--}60\text{S}^\circ$, $30\text{--}80\text{W}^\circ$) with Andes Mountains (Fig. 4c); and Antarctica ($60\text{--}90\text{S}^\circ$) (Fig. 4d). In all these regions, SubOro_NO simulates higher wind speeds than the ERA-Interim and the other two model runs. The effects of orography on wind speed are clearly reflected in both SubOro_OLD and SubOro_NEW runs, with the former having a stronger reduction of wind speed.

However, SubOro_NO performs better in terms of RMSE than SubOro_OLD in both the global view (Fig. 3) and in three out of four regions. Generally, as in Fig. 3, SubOro_NEW shows the best agreement with ERA-Interim.

Figure 5 shows the differences of global annual-mean 2-m temperature between the three model runs and Willmott and Matsuura surface air temperature (1950–1999). Again, we focus on the areas where terrain height standard deviation $\sigma > 0$. Over complex orography such as

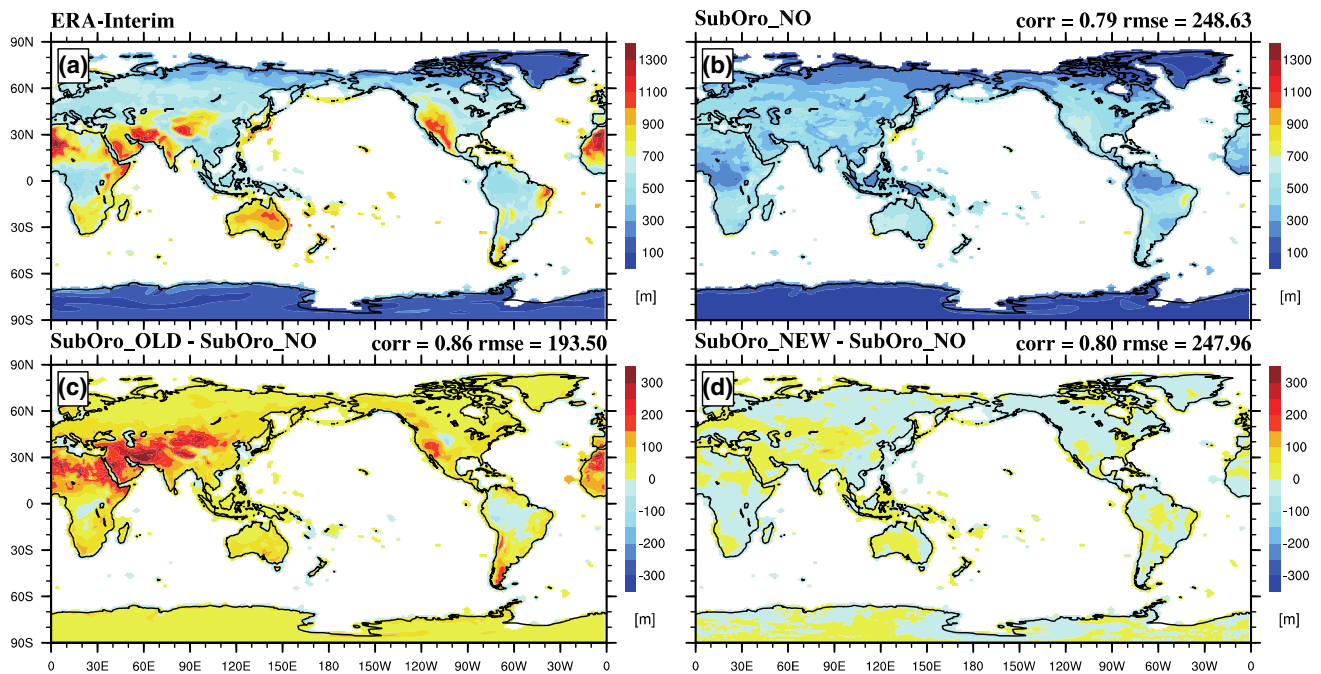


Fig. 6 Global annual-mean planetary boundary layer height (PBLH) over land ($\sigma > 0$) for **a** ERA-interim reanalysis and **b** SubOro_NO; **c** the difference between SubOro_OLD and SubOro_NO; and **d** the difference between SubOro_NEW and SubOro_NO

Tibetan Plateau, Rocky Mountains and Andes Mountains, both SubOro_NO and SubOro_NEW simulate a generally lower 2-m temperature than Willmott and Matsuura. Lower temperatures are also seen in the subtropical and tropical regions of the Northern Hemisphere. SubOro_OLD shows higher 2-m temperature over these areas, especially over Tibetan Plateau.

Figure 6 shows the global planetary boundary layer height (PBLH) of ERA-Interim, SubOro_NO over land areas and the differences between SubOro_OLD/SubOro_NEW and SubOro_NO. RMSEs and correlation coefficients of three models compared with ERA-Interim are also shown. SubOro_NO generally underestimate the PBLH compared with ERA-Interim reanalysis. The PBL in SubOro_OLD is deeper than in SubOro_NO by 200–400 m over the Northern Hemisphere in the subtropical and tropical regions by using indirect scheme, which is in better agreement with ERA-Interim. SubOro_NEW, however, has little change in PBLH compared with SubOro_NO, except showing an increased PBLH of 40–100 m over the Tibetan Plateau. As mentioned before, the indirect scheme TMS is used in the model's planetary boundary layer (PBL) scheme in SubOro_OLD, thus influences the PBL vertical transport and affects the PBL height. It enhances the vertical mixing and increases the PBLH over areas with complex terrain features. Although the BBW04 scheme has significant effects on simulating the low-level wind speed (Figs. 3, 4), its effect on boundary

layer vertical mixing is barely noticeable. The PBLH in ERA-Interim is a model parameter that is derived in terms of bulk Richardson number, which is modified to include the influence of thermals (Troen and Mahrt 1986), while CAM5 defines the PBLH using discrete levels (Lindvall et al. 2013). As in Lindvall et al. (2013), the PBLH simulated in CAM5 is underestimated compared to ERA-Interim over land and ocean.

Figure 7 shows the winter Northern Hemisphere 500 mb height differences between ERA-Interim and the three model runs. In both SubOro_OLD and SubOro_NEW, the negative geopotential height biases in SubOro_NO over Korean Peninsula and Japan are eliminated. There are two regions of positive biases over north Pacific in SubOro_NO while stronger biases appear in both SubOro_OLD and SubOro_NEW. SubOro_OLD also decreases the strong biases in SubOro_NO over north Atlantic while SubOro_NEW increases them. SubOro_OLD has the smallest RMSE of all. SubOro_NEW simulates worse results in 500 mb height than the other two runs compared to ERA-Interim. However, the differences between all three model runs and ERA-Interim are rather small compared to the large value of 500 mb height.

Figure 8 shows the seasonal variation of 10-m wind speed and 2-m temperature from ERA-Interim, NCEP2 wind speed, Willmott and Matsuura temperature. SubOro_NO, SubOro_OLD and SubOro_NEW averaged over global land and selected regions. The three model runs

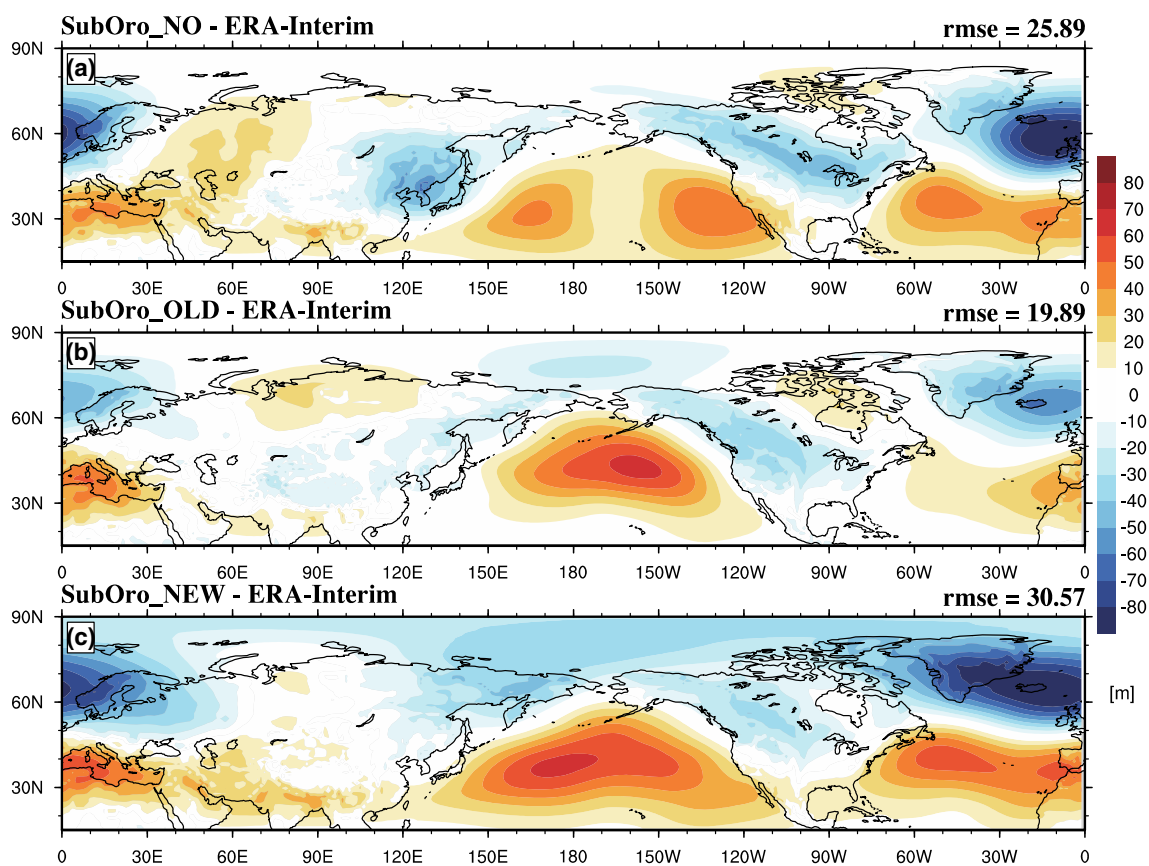


Fig. 7 The differences of north-hemisphere winter 500 mb height between **a** SubOro_NO, **b** SubOro_OLD, **c** SubOro_NEW and ERA-interim reanalysis

capture the seasonal variation of 10-m wind speed very well when comparing with the ERA-Interim data. Not surprisingly, SubOro_NO has the highest 10-m wind speed, SubOro_OLD has the lowest 10-m wind speed, and SubOro_NEW is in between for all seasons. SubOro_NEW is closest to ERA-Interim over all regions. The 10-m wind speed of NCEP2 reanalysis is generally more than 1.5 ms^{-1} smaller than that of ERA-Interim and the three model runs but shows similar seasonal variations on global average and over North and South America. For Asia, the 10-m wind speed in NCEP2 is smaller than in ERA-Interim except in December and January. For 2-m temperature, the three model runs simulate similar results over global and Asia, but have large differences over winter North America and summer South America. Large differences are seen in Northern Hemisphere winter between ERA-Interim and Willmott and Matsuura. The reason for this is unclear to us at this point. All three model runs and ERA-Interim overestimate the temperature over Global, Asia, North America and underestimate it over South America in all seasons compared with Willmott and Matsuura.

The diurnal cycles of wind stresses from three models are shown in Fig. 9 over complex terrains with $\sigma > 200$

in Asia ($0\text{--}60^\circ\text{N}$, $60\text{--}140^\circ\text{E}$), North America ($15\text{--}75^\circ\text{N}$, $60\text{--}140^\circ\text{W}$) and South America ($0\text{--}60^\circ\text{S}$, $30\text{--}80^\circ\text{W}$). We examined the total wind stresses and the contributions from both grid-scale surface roughness and subgrid-scale orography. SubOro_OLD simulates the strongest total wind stress all day, which agrees with the wind stress spatial distribution in Fig. 2. Although the total wind stress in SubOro_NEW is only slightly larger than that in SubOro_NO, it comes from different contributions. The grid-scale surface roughness contribution is larger in SubOro_NO than in SubOro_NEW. However, an extra contribution from subgrid orography in SubOro_NEW makes up most of the differences. In SubOro_OLD, the dominant contribution comes from subgrid orography whereas in SubOro_NEW grid-scale and subgrid-scale contributions are comparable. SubOro_NEW has a weaker diurnal variation than SubOro_OLD, which has a much stronger diurnal variation due to the fact that the indirect scheme TMS used in SubOro_OLD interacts strongly with boundary-layer stability.

As mentioned in the Introduction, besides using different subgrid orographic drag parameterization, SubOro_NEW uses a filtered orography, which is smoother and thus has smaller standard deviation of orographic heights

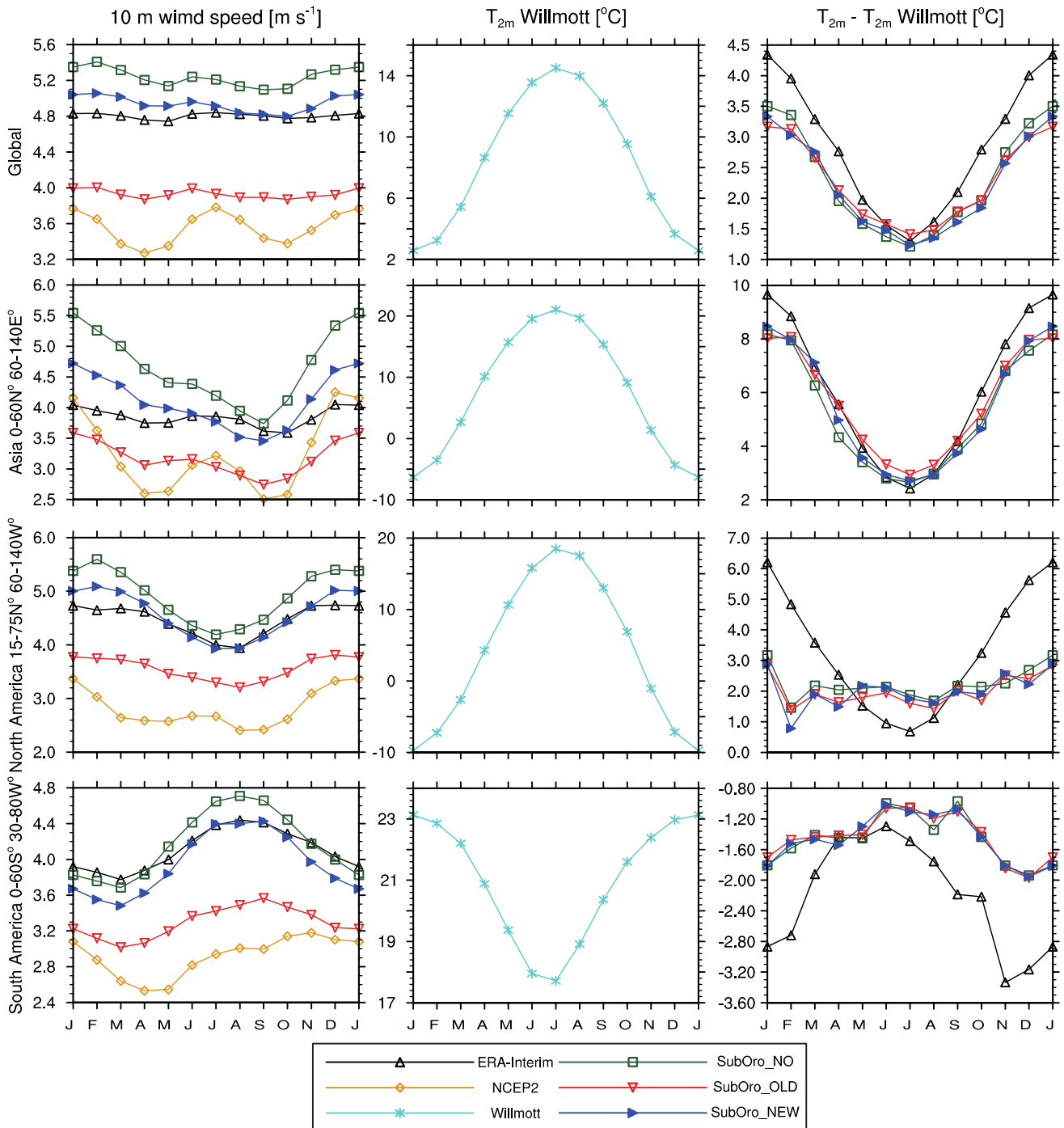


Fig. 8 Seasonal variability of 10-m wind speed and 2-m temperature over land ($\sigma > 0$) for ERA-interim reanalysis, NCEP2 reanalysis, Willmott and Matsuura surface air temperature, SubOro_NO, SubOro_OLD and SubOro_NEW

than in SubOro_OLD. To estimate the contribution of filtered orography data to the model simulation differences between SubOro_NEW and SubOro_OLD, we perform another experiment, SubOro_OLD_FLT, which uses the TMS scheme (from SubOro_OLD) and the filtered terrain height standard deviation data from SubOro_NEW.

Figure 10 shows the differences of wind stress and 10-m wind speed between SubOro_OLD_FLT and SubOro_OLD. The wind stress difference between SubOro_OLD_FLT and SubOro_OLD is generally smaller than 0.1 Nm^{-2} , which is rather small in magnitude. A difference of wind speed $< 0.5 \text{ ms}^{-1}$ is seen over most land areas except

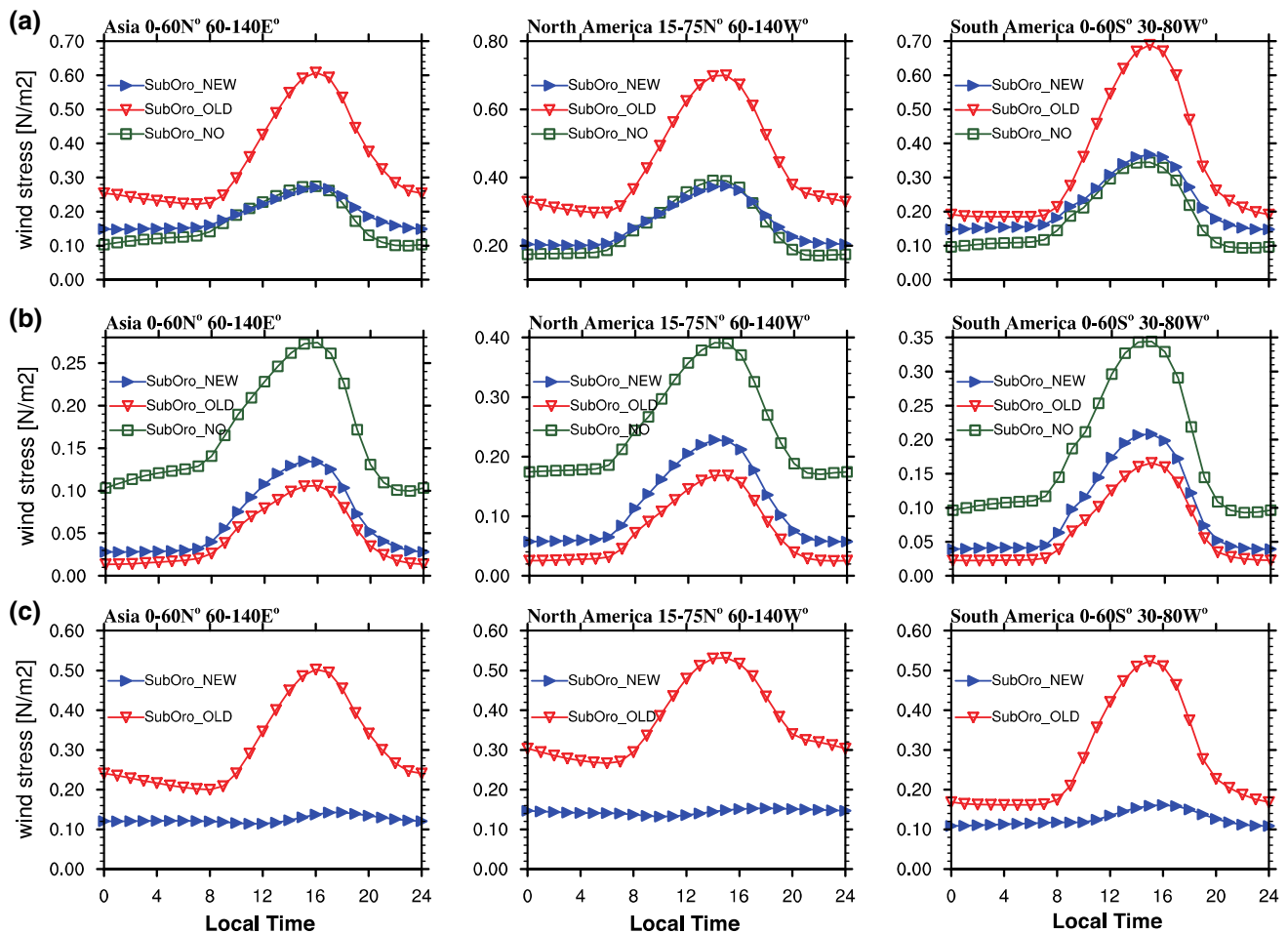


Fig. 9 The diurnal cycles of **a** total wind stresses, **b** the grid-scale orography and **c** subgrid-scale orography contribution for terrain height standard deviation $\sigma > 200$

Greenland and Antarctic. It is a non-negligible change, as SubOro_OLD mainly has annual mean wind speeds of between 1 and 4 ms^{-1} . However, 0.5 ms^{-1} is relatively small compared with the large differences between SubOro_OLD and SubOro_NEW. This affirms that the difference between SubOro_NEW and SubOro_OLD is mainly from the distinction between indirect and direct parameterization schemes. It is not clear to us what is the cause of the large difference over Greenland and Antarctic.

To further investigate the effect of subgrid orographic form drag on 10-m wind speed, we plot the probability distribution function (PDF) of the 10-m wind speed for the ERA-Interim and the four model runs in Fig. 11 over global land areas. PDFs are shown in regions where terrain height standard deviation $0 < \sigma < 100$, $100 < \sigma < 200$ and $\sigma > 200$ to see how orography affects the low-level wind speed. Over smooth orography ($0 < \sigma < 100$), the 10-m wind speed of SubOro_OLD is rather small compared with that of ERA-Interim. The peak of the PDF is around 1.5 ms^{-1} and probabilities of high wind speed are

relatively small. Large probabilities of high wind speed occurred in SubOro_NO and SubOro_NEW, for smooth orography causes little effects of subgrid drag in this case. The wind speed PDFs of ERA-Interim is similar to that of SubOro_NO and SubOro_NEW, but with higher high wind speed probabilities. As the orography becomes more complex, σ becomes greater. In the case of $100 < \sigma < 200$ and $\sigma > 200$, SubOro_NO still simulates a generally high 10-m wind speed. The wind speed of SubOro_OLD remains as small as 1.5 ms^{-1} when σ increases, except that the probabilities of high wind speed become even smaller. However, the probabilities of high wind speed in ERA-Interim and SubOro_NEW decrease quickly and clearly as the orography becomes more complex, with an increasing percentage of low wind speed as a consequence of the subgrid orography drag effects. The direct scheme BBW04 considers the subgrid turbulent orographic form drag as a forcing term in the equation of atmospheric motion. The effects of drag are accounted for directly in the model dynamic processes. This is the reason that ERA-Interim and SubOro_NEW has

Fig. 10 Differences of **a** surface wind stress and **b** 10-m wind speed between SubOro_OLD_FLT and SubOro_OLD over land ($\sigma > 0$)

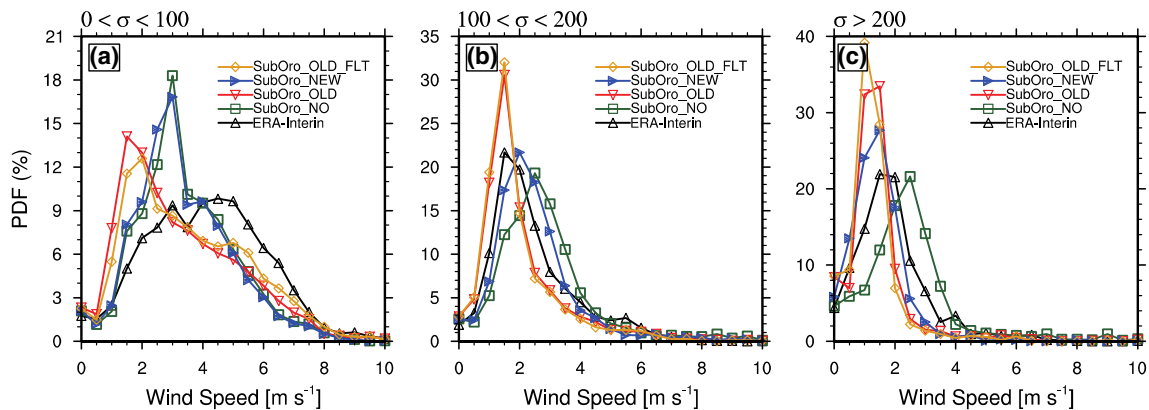
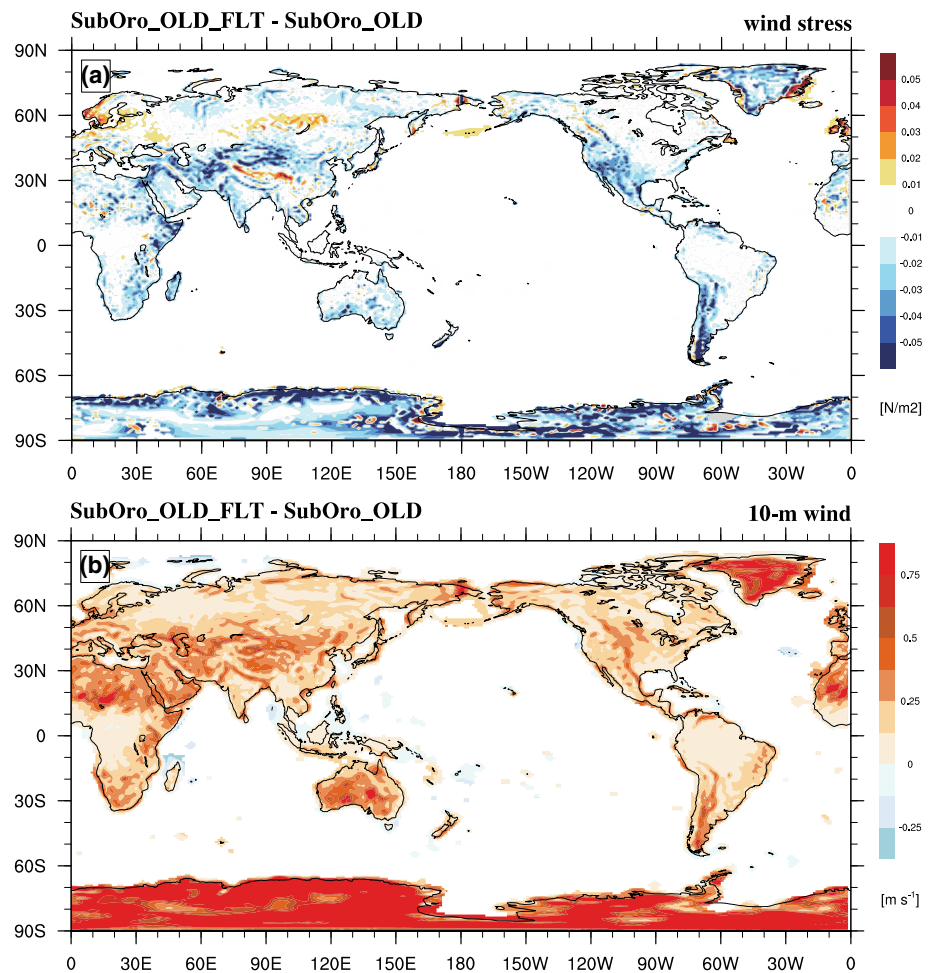


Fig. 11 The probability distribution function (PDF) of the 10-m wind speed for the ERA-Interim reanalysis, SubOro_NO, SubOro_OLD, SubOro_NEW and SubOro_OLD_FLT over global land areas when terrain height standard deviation **a** $0 < \sigma < 100$, **b** $100 < \sigma < 200$ and **c** $\sigma > 200$

more responses to complex orography than SubOro_OLD, which uses the indirect scheme and simulates a low wind speed even under relatively smooth orography. The global 10-m wind speed probability distribution of SubOro_OLD_FLT is much closer to that of SubOro_OLD than to

SubOro_NEW over both smooth and complex orography, which again confirms that the difference between SubOro_NEW and SubOro_OLD mainly comes from the distinction between two parameterization schemes but not the orography data.

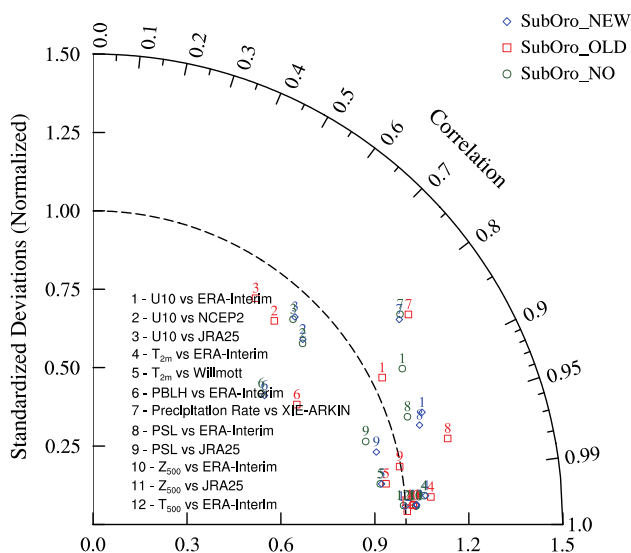


Fig. 12 Taylor diagram showing the overall performance of the three model runs compared with several reanalysis and observations

Figure 12 is a Taylor diagram showing the overall performance of the SubOro_NO, SubOro_OLD and SubOro_NEW. The statistics for the Taylor diagram are derived using: annual mean ERA-interim 10-m wind speed (U10), 2-m temperature (T_{2m}), PBLH, sea surface pressure (PSL), 500 mb height (Z_{500}) and 500 mb temperature (T_{500}); NCEP2 U10; JRA25 U10, PSL and Z_{500} ; Willmott and Matsuura T_{2m} and Xie-Arkin precipitation data. There are large differences in 10-m wind speed between parameterized models and SubOro_NO due to subgrid drag parameterizations. PSL differences between three models are also large. Differences in RMSE and correlation coefficients in 2-m temperature and precipitation are minor. PBLH of SubOro_OLD, same as Fig. 6 showed, agrees better with the ERA-Interim. The 500 mb height and temperature have little difference between three models.

4 Summary

We described and tested two parameterizations of subgrid-scale turbulent orographic form drag, the Turbulent Mountain Stress scheme (TMS) from default Community Atmosphere Model version 5 (CAM5) and the BBW04 scheme from Beljaars et al. (2004), using the NCAR Community Earth System Model version 1.0.4 (CESM1.0.4) global climate model. The TMS scheme represents turbulent drag as a drag coefficient, uses it to calculate the momentum flux in the surface layer, which influences the wind profiles in the upper layers through the vertical diffusion process. BBW04 considers turbulent drag as a direct effect on the atmospheric dynamic process by treating the drag

as a term in the equation of atmospheric motion. We conducted three sets of model experiments: one corresponding to the control and two corresponding to the different parameterization schemes. We compared the performance of these two schemes based on 10-m wind speed, 2-m temperature and planetary boundary layer height (PBLH). The BBW04 scheme produces a more similar result compared with ERA-Interim reanalysis when simulating 10-m wind speed. The TMS scheme increases the 2-m temperature and PBLH, not only over areas with complex terrain features, but also over large areas of sub-tropic and tropic in North Hemisphere.

Further analyses indicate that both indirect and direct schemes effectively reduce the low-level wind speed over land, but the latter one is more sensitive to complex orography. The contribution of filtered orography data was also considered. Smoother terrain has smaller subgrid orographic effects as expected. However, the effect of using smoother terrain in the BBW04 scheme is relatively small compared to the change of parameterization scheme from TMS to BBW04.

Acknowledgments This work was supported by funds from the Fundamental Research Funds for the Central Universities of China (Grant Nos. 110105016 and 110105018), the National Natural Science Foundation of China (Grant No. 41305121), and by the China Meteorological Administration Special Public Welfare Research Fund GYHY201406007.

References

- Allen T, Brown AR (2006) Modeling of turbulent form drag in convective conditions. *Bound Layer Meteorol* 118:421–429. doi:[10.1007/s10546-005-9002-z](https://doi.org/10.1007/s10546-005-9002-z)
- Belcher S, Wood N (1996) Form and wave drag due to stably stratified turbulent flow over low ridges. *Q J R Meteorol Soc* 122:863–902. doi:[10.1002/qj.49712253205](https://doi.org/10.1002/qj.49712253205)
- Belcher S, Newley T, Hunt J (1993) The drag on an undulating surface induced by the flow of a turbulent boundary layer. *J Fluid Mech* 249:557–596. doi:[10.1017/S0022112093001296](https://doi.org/10.1017/S0022112093001296)
- Beljaars ACM, Brown AR, Wood N (2004) A new parameterization of turbulent orographic form drag. *Q J R Meteorol Soc* 130:1327–1347. doi:[10.1256/qj.03.73](https://doi.org/10.1256/qj.03.73)
- Berrisford P, Dee D, Poli P, Brugge R, Fielding K, Fuentes M, Kallberg P, Kobayashi S, Uppala S, Simmons A (2011) The ERA-interim archive, version 2.0. ERA report series 1 technical report, ECMWF
- Brown AR, Wood N (2003) Properties and parameterization of the stable boundary layer over moderate topography. *J Atmos Sci* 60:2797–2808. doi:[10.1175/1520-0469\(2003\)060<2797:PAPOT>2.0.CO;2](https://doi.org/10.1175/1520-0469(2003)060<2797:PAPOT>2.0.CO;2)
- Fiedler F, Panofsky HA (1972) The geostrophic drag coefficient and the ‘effective’ roughness length. *Q J R Meteorol Soc* 415:213–220. doi:[10.1002/qj.49709841519](https://doi.org/10.1002/qj.49709841519)
- Gent PR, Danabasoglu G, Donner LJ, Holland MM, Hunke EC, Jayne SR, Lawrence DM, Neale RB, Rasch PJ, Vertenstein M, Worley PH, Yang Z, Zhang M (2011) The community climate system model version 4. *J Clim* 24:4973–4991. doi:[10.1175/2011JCLI4083.1](https://doi.org/10.1175/2011JCLI4083.1)

- Hunke EC, Lipscomb WH (2008) CICE: the Los Alamos sea ice model, documentation and software, version 4.0. Los Alamos National Laboratory Tech Rep LA-CC-06-012
- Hunt J, Leibovich S, Richards KJ (1988) Turbulent shear flows over low hills. *Q J R Meteorol Soc* 114:1435–1470. doi:[10.1002/qj.49711448405](https://doi.org/10.1002/qj.49711448405)
- Hurrell JW, Holland MM, Gent PR, Ghan S, Kay JE, Kushner PJ, Lamarque JF, Large WG, Lawrence D, Lindsay K, Lipscomb WH, Long MC, Mahowald N, Marsh DR, Neale RB, Rasch P, Vavrus S, Vertenstein M, Bader D, Collins WD, Hack JJ, Kiehl J, Marshall S (2013) The community earth system model: a framework for collaborative research. *Bull Am Meteorol Soc* 94:1339–1360. doi:[10.1175/BAMS-D-12-00121.1](https://doi.org/10.1175/BAMS-D-12-00121.1)
- IFS DOCUMENTATION-cy41r1, operational implementation, part IV: physical processes (2015) European Centre for Medium-Range Weather Forecast, Shinfield Park, Reading, RG2 9AX, England
- Jackson PS, Hunt J (1975) Turbulent wind flow over a low hill. *Q J R Meteorol Soc* 101:929–955. doi:[10.1002/qj.49710143015](https://doi.org/10.1002/qj.49710143015)
- Lawrence DM, Oleson KW, Flanner MG, Thornton PE, Swenson SC, Lawrence PJ, Zeng X, Yang Z, Levis S, Sakaguchi K, Bonan GB, Slater AG (2011) Parameterization improvements and functional and structural advances in version 4 of the community land model. *J Adv Model Earth Syst* 3:M03001. doi:[10.1029/2011MS000045](https://doi.org/10.1029/2011MS000045)
- Lindvall J, Svensson G, Hannay C (2013) Evaluation of near-surface parameters in the two versions of the atmospheric model in CESM1 using flux station observations. *J Clim* 26:26–44. doi:[10.1175/JCLI-D-12-00020.1](https://doi.org/10.1175/JCLI-D-12-00020.1)
- Milton SF, Wilson CA (1996) The impact of parametrized sub-grid-scale orographic forcing on systematic errors in a global NWP model. *Mon Weather Rev* 124:2023–2045. doi:[10.1175/1520-0493\(1996\)124<2023:TIOPSS>2.0.CO;2](https://doi.org/10.1175/1520-0493(1996)124<2023:TIOPSS>2.0.CO;2)
- Neale RB, Chen C, Gettelman A, Lauritzen PH, Park S, Williamson DL, Conley AJ, Garcia R, Kinnison D, Lamarque J, Marsh D, Mills M, Smith AK, Tilmes S, Morrison H, Cameron-Smith P, Collins WD, Iacono MJ, Easter RC, Ghan SJ, Liu X, Rasch PJ, Tayloy MA (2010) Description of the NCAR community atmosphere model (CAM 5.0). NCAR tech note TN-486
- Richter J, Sassi F, Garcia RR (2010) Toward a physically based gravity wave source parameterization in a general circulation model. *J Atmos Sci* 67:136–156. doi:[10.1175/2009JAS3112.1](https://doi.org/10.1175/2009JAS3112.1)
- Rontu L (2006) A study on parameterization of orography-related momentum fluxes in a synoptic-scale NWP model. *Tellus* 58A:69–81. doi:[10.1111/j.1600-0870.2006.00162.x](https://doi.org/10.1111/j.1600-0870.2006.00162.x)
- Smith RD, Jones P, Briegleb B, Bryan F, Danabasoglu G, Dennis J, Dukowicz J, Eden C, Fox-Kemper B, Gent P, Hecht M, Jayne S, Jochum M, Large W, Lindsay K, Malturb M, Norton N, Peacock S, Vertenstein M, Yeager S (2010) The parallel ocean program (POP) reference manual: ocean component of the community climate system model (CCSM) and community earth system model (CESM). Los Alamos National Laboratory Tech Rep LAUR-10-01853
- Sykes RI (1980) An asymptotic theory of incompressible turbulent flow over a small hump. *J Fluid Mech* 101:647–670. doi:[10.1017/S002211208000184X](https://doi.org/10.1017/S002211208000184X)
- Troen I, Mahrt L (1986) A simple model of the atmospheric boundary layer: sensitivity to surface evaporation. *Bound Layer Meteorol* 37:129–148. doi:[10.1007/BF00122760](https://doi.org/10.1007/BF00122760)
- Webster S, Brown AR, Cameron DR, Jones P (2003) Improvements to the representation of orography in the met office unified model. *Q J R Meteorol Soc* 129:1989–2010. doi:[10.1256/qj.02.133](https://doi.org/10.1256/qj.02.133)
- Willmott CJ, Robeson SM (1995) Climatologically aided interpolation (CAI) of terrestrial air temperature. *Int J Climatol* 15:221–229. doi:[10.1002/joc.3370150207](https://doi.org/10.1002/joc.3370150207)
- Wilson JD (2002) Representing drag on unresolved terrain as a distributed momentum sink. *J Atmos Sci* 59:1629–1637. doi:[10.1175/1520-0469\(2002\)059<1629:RDOUTA>2.0.CO;2](https://doi.org/10.1175/1520-0469(2002)059<1629:RDOUTA>2.0.CO;2)
- Wood N, Mason P (1993) The pressure force induced by neutral, turbulent flow over hills. *Q J R Meteorol Soc* 119:1233–1267. doi:[10.1002/qj.49711951402](https://doi.org/10.1002/qj.49711951402)
- Wood N, Brown AR, Hewer FE (2001) Parameterizing the effects of orography on the boundary layer: an alternative to effective roughness lengths. *Q J R Meteorol Soc* 127:759–777. doi:[10.1002/qj.49712757303](https://doi.org/10.1002/qj.49712757303)
- Xie P, Arkin PA (1997) Global precipitation: a 17-year monthly analysis based on gauge observations, satellite estimates, and numerical model outputs. *Bull Am Meteorol Soc* 78:2539–2558. doi:[10.1175/1520-0477\(1997\)078<2539:GPAYMA>2.0.CO;2](https://doi.org/10.1175/1520-0477(1997)078<2539:GPAYMA>2.0.CO;2)
- Xue H, Shen X, Su Y (2011) Parameterization of turbulent orographic form drag and implementation in GRAPES. *J Appl Meteorol Sci* 22(2):169–181